Geometrically isomeric [Ir(iqbt)(ppy)(hpa)] complexes with differential molecule orientations for efficient near-infrared (NIR) polymer light-emitting diodes (PLEDs)

Wentao Li, [‡,a] Jiaxiang Liu,[‡,a] Baowen Wang,[a] Siyu Hou,[a] Xingqiang Lü,*[a] Guorui Fu*[a,b] and Wai-Yeung Wong*[b]

[a]*School of Chemical Engineering, Northwest University, Xi'an 710069, Shaanxi, China. E-mail: lvxq@nwu.edu.cn*

[b]*Department of Applied Biology and Chemical Technology, The Hong Kong Polytechnic University, Hung Hom, Hong Kong, China. E-mail: guorui.fu@polyu.edu.hk; wai-yeung.wong@polyu.edu.hk*

Based on the geometrical isomerisation to the [Ir(C^N^1)(C^N^2)(N^O))-*tris*-heteroleptic Ir(III)-complexes, the augmented transition dipole transition (TMD) with a preferentially horizontal orientation, beneficial for their photo-excited and electroluminescent NIR-phosphorescence, is reported.

Contributing from the iridium(III)-induced strong spin-orbital coupling[1] that allows fast singlet-triplet intersystem crossing (ISC), neutral cyclometalated Ir(III)-complexes featuring good thermal/electrochemical stability, high luminous efficiency and rather short phosphorescence lifetime, endow the most promising potential to organic/polymer light-emitting diodes (OLEDs/PLEDs).[2] Moreover, associated with ^{3}LC/^{3}MLCT-admixed (LC = ligand-centred, MLCT = metal-to-ligand charge transfer) transitions in the ^{1}T excited state, their emissive colours can be flexibly modulated across the whole visible regime (from near-UV to visible and to near-infrared (NIR, λ_{em} > 690 nm)) through ligands' specific engineering.[3] For typical neutral iridium(III)-complexes towards reliable OLEDs/PLEDs, in dependence on the differential ligand (0/-1/-2; neutral or anionic) number, conventional [Ir(C^N)$_3$][4]/[Ir(C^C)$_3$][5]-homoleptic (-1,-1,-1) complexes with three identical C^N/C^C-ligands and [Ir(C^N)$_2$(L^X)][6]/[Ir(C^C)$_2$(L^X)][7]-*bis*-heteroleptic (-1,-1,-1; L^X = C'^N', O^O, N^O or N^N, etc.) complexes with two identical C^N/C^C-ligands and one L^X-ancillary ligand, together with recently renovated *tris*-heteroleptic-type (-1,-1,-1; [Ir(C^N^1)(C^N^2)(O^O)],[8] [Ir(C^N^1)(C^N^2)(C^N^3)],[9] [Ir(C^N)(N^N^1)(N^N^2)],[10] [Ir(C^N^1)(C^N^2)(C^C)][11] or [Ir(C^N^1)(C^N^2)(N^O)][12]; -2,-1,0, [Ir(C^C)(C^N)(N^N)][13]) analogue composed of one Ir(III) ion and three different ligands, were developed, respectively. In comparison, despite the structural diversity to the *tris*-heteroleptic-counterpart for appreciable vivid-visible (λ_{em} = 465-669 nm) OLEDs/PLEDs,[8-11,13] it is very rare[12] and remains a great challenge[14] to extend the gamut into the NIR regime and to achieve high-efficiency NIR-OLEDs/PLEDs limited by the so-called "energy gap law".[15]

Undoubtedly, another challenge, to a certain extent, should be attributed to the isomeric complexity for homoleptic, *bis*-heteroleptic or *tris*-heteroleptic-type. On one hand, apart from the classical Ir(III)-complex isomers arisen from different HC^N/HC^C and/or HL^X ligands with structure[16] or *R*/*S*-chirality isomerism,[17] the octahedral configuration of Ir(III)-centre engenders *Λ*- (left-handed propeller) and *Δ*-optical (right-handed propeller) isomers[18] for one neutral Ir(III)-complex species, in which their metal-centred stereogenic separation is substantially accessible from chiral supercritical fluid chromatography. On the other hand, even without considering the enantiomeric resolution mentioned above, multi-ligands' differential alignment engenders the N,N,N-facial/meridional (C_3-axial-*fac*/C_1-axial-*mer*) geometrical isomers[19-20] in a racemic mixture. In other kind, arising from the O^O-restrictive symmetry (such as acac, etc.), this phenomenal methodology is evidently invalid to its C_2-symmetric [Ir(C^N)$_2$(O^O)]-*bis*-heteroleptic form.[21] Noticeably, as for asymmetric-L^X-induced [Ir(C^N)$_2$(L^X)]-*bis*-heteroleptic racemate with C_1-symmetry, the N^N-*cis*/*trans*-positional diversity of two identical C^N ligands gives rise to additional stereoisomers within the *mer*-type, from which, geometrical isomerism to the *tris*-heteroleptic-system should be more plentiful. To simplify it for an explicit statement, geometrical isomerism in racemates to [Ir(C^N)$_3$]-homoleptic, [Ir(C^N)$_2$(N'^O)]-*bis*-heteroleptic and [Ir(C^N)(C'^N')(N''^O)]-*tris*-heteroleptic neutral (-1,-1,-1) Ir(III)-complexes is focused (**Scheme 1**) for discussion. Inclusively as a universal rule[22] to the kinetically favoured N,N,N-*mer*-[Ir(C^N)]$_3$ while the thermodynamically favoured for the N,N,N-*fac*-[Ir(C^N)]$_3$, the *mer*-isomer was demonstrated to thermally or photo-chemically convert to the more stable *fac*-counterpart with more attractive photo-physical and electroluminescent properties. As to the asymmetric-N^O induced C_1-symmetric [Ir(C^N)$_2$(N'^O)]-*bis*-heteroleptic species, four kinds of stereoisomers (C,C-*cis*-and-N,N-*cis* for the N,N,N'-*fac*-form, C,C-*cis*-and-N,N-*cis*, C,C-*cis*-and-N,N-*trans* and C,C-*trans*-and-N,N-*cis* for the N,N,N'-*mer*-type; see **Scheme 1**) can be theoretically predicted, while two[23] or three[24] isomeric racemates were isolated and structurally confirmed. For the C_1-symmetric-[Ir(C^N)(C'^N')(N''^O)]-*tris*-heteroleptic system, the combination of N,N',N''-*fac*/*mer* and C^C'/N^N'-*cis*/*trans* cases gives two C,C'-*cis*-and-N,N'-*cis* geometrical isomers in the N,N',N''-*fac*-form and six possible geometrical isomers (see **Scheme 1**) within the N,N',N''-*mer*-type. Unfortunately, among the previously

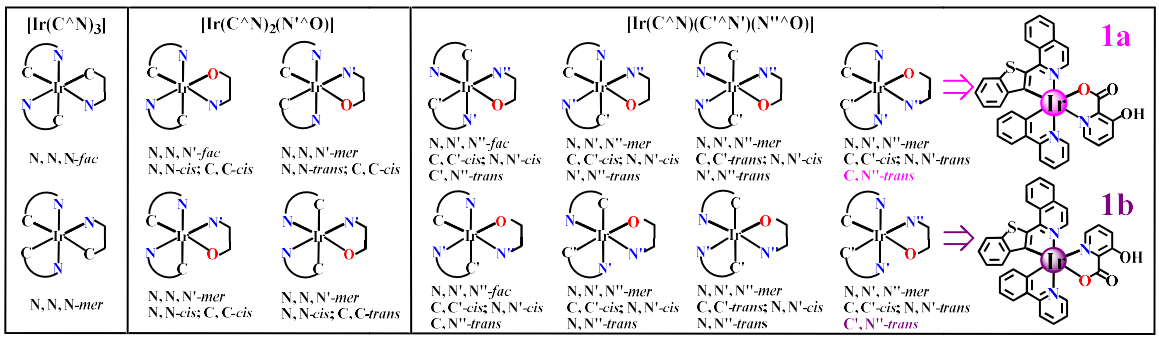

Scheme 1 Structural scheme of geometrical isomers of [Ir(C^N)$_3$]-homoleptic, [Ir(C^N)$_2$(N^O)-*bis*-heteroleptic or [Ir(C^N)(C'^N')(N''^O)]-*tris*-heteroleptic Ir(III)-complexes including **1a** and **1b**.

reported *tris*-heteroleptic Ir(III)-complexes,[8-13] just one racemic species characteristic of the C,C-*cis*-and-N,N-*trans* and/or N,N',N''-*mer*-form was isolated and used for the doped OLEDs/PLEDs.

Along with the geometrically isomeric racemate cognition on typical [Ir(C^N)$_3$]-homoleptic and [Ir(C^N)$_2$(L^X)]-*bis*-heteroleptic neutral species, the C_3- to C_2/C_1-symmetrical effect on the specific orientation of their transition dipole moment (TDM) vectors was highlighted.[25] Importantly, based on the empirical out-coupling verification of the preferential molecule orientation, visible-OLEDs (λ_{em} < 600 nm)[26] from C_2/C_1-symmetrical Ir(C^N)$_2$(L^X)]-heteroleptic Ir(III)-complexes were realized to have significantly higher light-extracting efficiencies (η_{out}) compared to the *fac*-[Ir(C^N)$_3$]-homoleptic C_3-analogs.[27] In light of the substantially lowest symmetry of *tris*-heteroleptic neutral Ir(III)-complexes with three different ligands, herein, it is of interest to extend this structure-designed strategy from the visible-light (λ_{em} = 465-669 nm)[8-11,13] into the NIR-emission (λ_{em} > 690 nm) for affording our novel [Ir(C^N^1)(C^N^2)(N^O)]-*tris*-heteroleptic Ir(III)-complexes **1a** and **1b** (see **Scheme 1**): i) correlation between molecule orientation and geometrical isomerism (like **1a** and **1b**, etc.) is never specifically explored for *tris*-heteroleptic neutral Ir(III)-complexes; ii) challenging the so-called "energy gap law"[15] with unsatisfactory efficiencies of NIR-OLEDs/PLEDs based on the reported *fac*-[Ir(C^N)$_3$]-homoleptic[28] and [Ir(C^N)$_2$(L^X)]-*bis*-heteroleptic[29] NIR-emitters, it is expected that a preferentially horizontal orientation could be motivated to enhance the NIR-light extraction from the **1a**/**1b**-*tris*-heteroleptic geometrical isomerism.

The one-pot synthetic strategy to **1a**/**1b** is depicted in the ESI and **Scheme S1**. That is, through metalation of equimolar **Hiqbt** as the HC^N^1 ligand and **Hppy** as the HC^N^2 ligand with $IrCl_3 \cdot 3H_2O$ and the subsequent treatment with **Hhpa** in the presence of *t*-BuOK, the [Ir(C^N^1)(C^N^2)(N^O))-*tris*-heteroleptic isomers (**1a** and **1b**) together with the [Ir(C^N)$_2$(N^O)-*bis*-heteroleptic by-products ([Ir(ppy)$_2$(hpa)] and [Ir(iqbt)$_2$(hpa)]) were concurrently formed with acceptable yields. Depending on the polarity-different chromatography approach, the four Ir(III)-complexes, while with no other isomeric forms, were eluted, respectively. Apart from the identification confirmed by EA, FT-IR and ESI-MS (ESI), ^{1}H NMR results (**Figure S1**) of the stipulated 1:1:1 integration ratio between the (**iqbt**)$^-$/(**ppy**)$^-$/(**hpa**)$^-$ proton signals verify the identical [Ir(C^N^1)(C^N^2)(N^O))-*tris*-heteroleptic component for isomers **1a** and **1b**. Noticeably, a significantly broadened (δ = 13.77-6.04 ppm) proton resonances for **1a** in relative to those (δ = 13.61-6.20 ppm) for **1b** should be caused by the (**hpa**)$^-$-induced different multi-ligands alignment. The molecular structures of **1a**·$CHCl_3$ and **1b** were further deduced from X-ray diffraction data (**Tables S1-2**), as shown in **Figure 1**. The (**iqbt**)$^-$-C^N^1 and (**ppy**)$^-$-C^N^2 ligands configure with the usual C,C-*cis*-and-N,N-*trans* chelating mode, the (**hpa**)$^-$-N^O *syn*/*anti*-positional difference makes **1a** and **1b** geometrically stereoisomeric with the *mer*-type racemates.[30] Meanwhile, their similar thermal stability (**Figure S2**) with a decomposition (5 wt% loss) temperature over 310 °C is sufficiently enough to the device fabrication.

The photo-physical property of **1a** and **1b** in degassed CH_2Cl_2 solutions are shown in **Table S3** and **Figure 2**. In comparison, the absorptions of the two geometrical isomers are nearly identical, where the UV bands (λ_{ab} < 400 nm) should be assigned to the ligand-based π-π* transitions **(Figures S3-4)** and the visible bands (λ_{ab} > 420 nm) from the LC/MLCT-mixed transitions. When excited within the absorption-wide region (λ_{ex} = 375 nm) at 298 K, their close similarity is reflected with the almost identical while exclusive NIR-emissions (peaking at 697 nm and a shoulder at 756 nm for **1a**; 696 nm and 760 nm for **1b**; versus 700 nm and 760 nm for [Ir(iqbt)$_2$(hpa)] (**Figure S5**) while visible-emissions (**Figure S6**) of the ligands or [Ir(ppy)$_2$(hpa)]) and equivalent Huang-Rhys factors (S_M; 0.32-0.34) with efficient Dexter[31] energy transfer. Meanwhile, even at 77 K, these NIR-emissive parameters (**Figure S7** and **Table S3**) are well maintained, indicating a robust geometry configuration for the two stereoisomers. However, despite the comparable NIR-phosphorescent lifetime (τ = 0.33 μs (**1a**) or 0.38 μs (**1b**) time-decayed at λ_{em} = 697 nm), the multi-ligands' alignment difference between **1a** and **1b**, engenders the relatively higher Φ_{PL} (0.33) for **1b** than that (0.27) of **1a**, which is in good agreement with the larger k_r (8.7×10^5 s^{-1} versus 8.2×10^5 s^{-1} (**1a**)) but smaller k_{nr} (1.8×10^6 s^{-1} versus 2.2×10^6 s^{-1} (**1a**)) for **1b**. Interestingly, owing to the symmetry breaking of the [Ir(iqbt)(ppy)(hpa)]-**1a**/**1b** with C_1-symmetry relative to the C_3-symmetric *fac*-[Ir(iqbt)$_3$][28] or C_2-symmetric [Ir(iqbt)$_2$(L^X)]-counterpart,[29d-29e] the significantly higher Φ_{PL} (0.27-0.33) is accompanied with the relatively shorter lifetime (τ = 0.33-0.38 μs) compared to those (τ ~ 1.0 μs and Φ_{PL} = 0.07-0.19) of the *fac*-[Ir(iqbt)$_3$]/ [Ir(iqbt)$_2$(L^X)]-species.

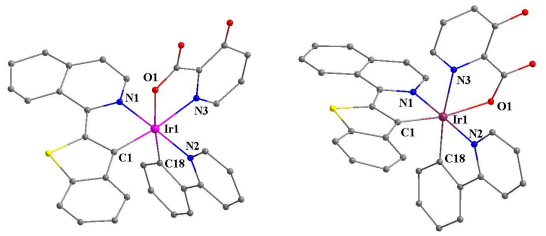

Figure 1 The [Ir(C^N)(C'^N')(N''^O)]-*tris*-heteroleptic mononuclear framework for geometrical isomers **1a**·$CHCl_3$ (left) and **1b** (right); H atoms, most labels and/or solvate are omitted for clarity.

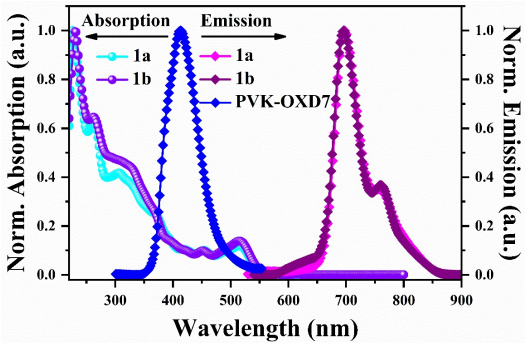

Figure 2 The normalized UV-visible absorption and emission (λ_{ex} = 375 nm) spectra of **1a** and **1b** in degassed CH_2Cl_2 solutions or PVK-OXD7 in solid-state (λ_{ex} = 273 nm) at room temperature.

To further understand the photo-physical property of **1a** and **1b**, DFT/TD-DFT calculations were explored with the detailed data summarized in **Tables S4-5/Figure S8-9**. On one hand, due to the geometrical isomerism between **1a** and **1b**, the (**hpa**)$^-$-portion in **1b** has the slightly larger electron contribution (3.66%) to the HOMO than that (2.76%) in **1a**, while the significantly differential distributions (51.74% from the (**iqbt**)$^-$, 29.40% from the Ir(III) and 15.20% from the (**ppy**)$^-$ for **1b** versus the corresponding 63.28%, 24.29% and 9.68% for **1a**) are observed. Accordingly, besides the similar main contribution (89.39% (**1a**) versus 92.51% (**1b**) from the (**iqbt**)$^-$ while the negligible (0.35-0.40%) one from the (**ppy**)$^-$to the LUMO, the slightly larger contribution (5.16%) from the Ir(III) for **1b** than that (4.54%) for **1a** is compensated with the evident reduction (1.94% (**1b**) versus 5.72% (**1a**)) from the (**hpa**)$^-$. However, in sharp contrast to the concurrent stabilization of HOMO/LUMO level (-4.88/-1.93 eV) for **1b** relative to **1a** (-4.81/-1.82 eV), their HOMO-LUMO bandgaps (2.95 eV (**1b**) versus 2.99 eV (**1a**)) are comparable. On the other hand, contributing from the most (94.1% (**1a**) versus 92.9% (**1b**)) contribution from the HOMO → LUMO transition to the corresponding ^{1}T state characteristic of the similar ^{3}LC/^{3}MLCT-mixed transitions, the almost equivalent (2.67 eV (**1a**) versus 2.63 eV (**1b**)) ^{1}T-energy should be reason to their nearly identical NIR-phosphorescence. Evidently, the more strengthened ^{3}MLCT effect (19.73%) in **1b** than that (16.68%) of **1a** is beneficial for the relatively higher Φ_{PL} for **1b** than that of **1a**.

For the deep clarification of differential NIR-emissive efficiencies between **1a** and **1b**, the dipole moment vectors of $\vec{\mu}$-^{0}S, $\vec{\mu}$-^{1}T and $\Delta\vec{\mu}$-(^{1}T→^{0}S) were calculated by DFT, and summarized in **Table S6/Figure 3**. In contrast to the $\vec{\mu}$-^{0}S/^{1}T/^{1}T→^{0}S directions located at the C_2-axis of typical C_2-symmetrical [Ir(C^N)$_2$(L^X)]-*bis*-heteroleptic Ir(III)-complexes, the θ angles (11.85° (**1a**) versus 19.21° (**1b**)) between $\vec{\mu}$-^{0}S and $\vec{\mu}$-^{1}T for the two isomers with the C_1-

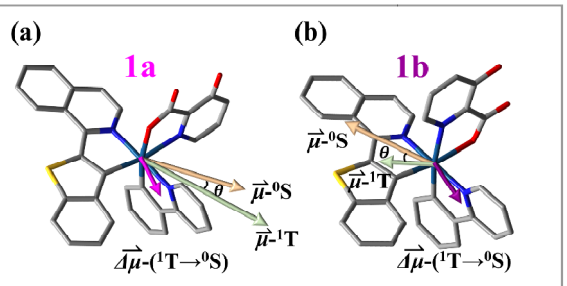

Figure 3 The dipole moment vectors of $\vec{\mu}$-^{0}S, $\vec{\mu}$-^{1}T and $\Delta\vec{\mu}$-(^{1}T→^{0}S) for the isomers **1a** (left) and **1b** (right) based on their corresponding optimized S_0 and T_1 geometries.

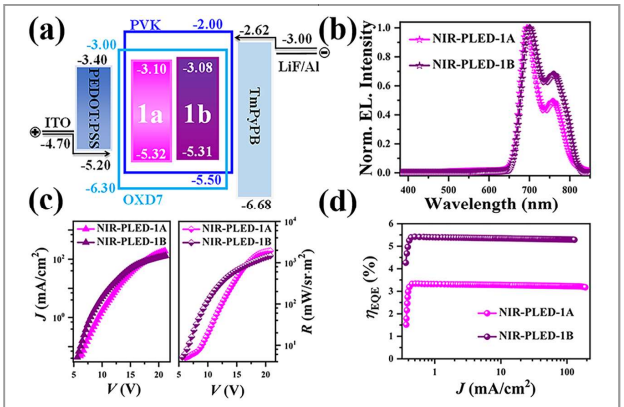

Figure 4 (a) Device structures and energy level diagrams; (b) the electroluminescent spectra; (c) the current density (*J*) and radiance (*R*) as a function of applied voltage (*V*); (d) and the external quantum efficiency η_{EQE} versus *J* curves for the **NIR-PLEDs-1A/1B**.

symmetry are different. Moreover, despite the relatively smaller $\vec{\mu}$-^{0}S and $\vec{\mu}$-^{1}T sizes (6.75 and 6.53 D) for **1b** than those (7.62 and 8.58 D) of **1a**, the TDM value (2.23 D; $\Delta\vec{\mu}$-(^{1}T→^{0}S)) of **1b** is larger than that (1.92 D) of **1a**. Referring to the so-called "energy-gap law",[15] apart from k_{nr} inversely exponential and k_r cubicly dependent on the ^{1}T level, k_r is concurrently proportional to the square of the TDM according to the electronic transition theory.[32] Therefore, the larger TDM generated for **1b**, is in favour of the fast radiative transition, reasoning for the more efficient nature than **1a** especially with the identical ^{1}T energy. For sure, the effect of TDM on the molecular orientation of their-doped EMLs needs to be further verified (*vide infra*).

Thanks to PVK-OXD7 (65:30; wt%) with good hole/electron transport for being a suitable *co*-host,[12,29] it is especially interesting to use the geometrical isomers **1a** and **1b** as the dopants for their solution-processed **NIR-PLEDs-1A/1B** with the same configuration shown in **Figure 4(a)/Table S7**. On one hand, based on the electrochemical result (**Figure S10**), the experimental HOMO/LUMO levels of -5.32/-3.10 eV for **1a** or -5.31/-3.08 eV for **1b** are located within the bandgap of the *co*-host, and thus, the injected electrons/holes through the *co*-host should be trapped and recombined within the NIR-emitters **1a**/**1b**. On the other hand, contributing from the significant spectral overlap (also **Figure 2**) between the emission of PVK-OXD7 and the LC/MLCT-based absorption of **1a** or **1b**, effective Förster[33] energy transfer from the *co*-host to the dopant together with efficient Dexter[31] energy transfer could be motivated. Just as expected, the normalized electroluminescent spectra (**Figure 4(b)**) resemble the corresponding photo-luminescent profiles and are independent of the applied voltages (**Figure S11**), indicating that valid Förster/Dexter energy transfers occurr during the charge-trapping process. Moreover, along with the monotonous increase (**Figure 4(c)** of the *J*/*R* upon increasing the applied bias voltage, the η_{EQE} (**Figure 4(d)**) in each case increases instantly and then decreases steadily throughout the whole illumination. However, in contrast to the larger R^{Max} of 1952.9 mW/sr·m^2 for the **NIR-PLED-1A** than 1499.0 mW/sr·m^2 for the **NIR-PLED-1B** at the cost of the higher J^{Max} (191.5 mA/cm^2 versus 130.8 mA/cm^2), the η_{EQE}^{Max} of 5.4% for the **NIR-PLED-1B** is significantly larger than that (3.3%) for the **NIR-PLED-1A**. Evidently, besides the similarly negligible efficiency roll-off (< 5%) throughout the whole illumination, the 1.6-fold increase of η_{EQE}^{Max} for the **NIR-PLED-1B** compared to the **NIR-PLED-1A**, is not consistent with the Φ_{PL} trend (Φ_{PL} of 0.33 for **1a** versus 0.27 for **1b**).

By following the nearly compatible energy-level alignment with the same device-architecture,[12,29d] the effect of comparable η_h on the differential η_{EQE}^{Max} for the **NIR-PLEDs-1A/1B** could be reasonably ignored. Therefore, the different NIR-light out-coupling (η_{out}) arising from the specific molecular orientation for the geometrical isomer **1a** or **1b** should be another decisive factor.

To confirm this hypothesis, the orientation distribution of the two emitting layers (EML-**1a**/EML-**1b**) for the **NIR-PLEDs-1A/1B** was quantitatively checked by variable-angle spectroscopic ellipsometry (VASE) method with the results shown in **Table S8**/**Figure S12**. In accompany with the ordinary/extraordinary coefficients for the EML-**1a**/EML-**1b**, the corresponding order parameter *S* of -0.09 for the EML-**1a** or -0.14 for the EML-**1b** is calculated. Accordingly, in contrast to the isotropic case with *S* = 0, the horizontal dipole ratio (*h*/(*h*+*v*); 72.0% of the EML-**1a** versus 76.0% of the EML-**1b** is realized. Noticeably, the more preferential orientation parallel to the substrate of the EML-**1b** than that of the EML-**1a**, should be also positively beneficial to the higher efficiency (η_{out}-**1B**/η_{out}-**1A** = 1.3; η_{EQE}-**1B**/η_{EQE}-**1A** = 1.6) of the **NIR-PLED-1B** compared to the **NIR-PLED-1A**. Encouragingly, the highest η_{EQE}^{Max} of 5.4% for the **NIR-PLED-1B** among the previous solution-processed NIR-OLEDs/PLEDs and even the top-level within the vacuum-deposited NIR-OLEDs based on Ir(III)-complexes,[12,28-29] shows that the [Ir(C^N^1)(C^N^2)(N^O))-*tris*-heteroleptic Ir(III)-complexes especially with an interesting geometrical isomerisation, should be promising candidates for future low-cost scalable NIR-PLEDs.

In conclusion, through the geometrically isomeric design to the [Ir(C^N^1)(C^N^2)(N^O))-*tris*-heteroleptic Ir(III)-complexes **1a** and **1b** with NIR-phosphorescence, the augmented TMD with a preferentially horizontal orientation, beneficial for both the photo-excited and electroluminescent property, is observed.

This work was supported by the NSFC (21373160, 21173165, 51873176), the State Key Laboratory of Structure Chemistry (20190026), the Hong Kong Research Grants Council (PolyU153058/19P), the Hong Kong Polytechnic University (1-ZE1C and YW4T) and the Endowed Professorship in Energy from Ms. Clarea Au (847S).

Notes and references

1. A. F. Henwood and E. Zysman-Colman, *Chem. Commun.*, 2017, **53**, 807-826.
2. E. Longhi and L. De Cola, Hogan, *Iridium(III) in Optoelectronic and Photonic Applications*, Wiley-VCH: Weineim, Germany, 2017, **1**, 359-414.
3. T. Y. Li, J. Wu, Z. G. Wu, Y. X. Zheng, J. L. Zuo and Y. Pan, *Coord. Chem. Rev.*, 2018, **374**, 55-92.
4. Y. Bin Mohd, R. Abd, A. J. Huckaba and M. K. Nazeeruddin, *Top. Curr. Chem.*, 2017, **375**, 1-30.
5. I. Omae, *Coord. Chem. Rev.*, 2016, **329**, 191-213.
6. T. Tsuboi and W. Huang, *Israel J. Chem.*, 2014, **54**, 885-896.
7. A. Bonfiglio and M. Mauro, *Eur. J. Inorg. Chem.*, 2020, **36**, 3427-3442.
8. X. L. Yang, H. R. Guo, B. A. Liu, J. Zhao, G. J. Zhou, Z. X. Wu and W.-Y. Wong, *Adv. Sci.,* 2018, **5**, 1701067.
9. W. P. Dang, X. L. Yang, Z. Feng, Y. H. Sun, D. K. Zhong, G. J. Zhou, Z. X. Wu and W.-Y. Wong, *J. Mater. Chem. C.,* 2018, **6**, 9453-9464.
10. J.-L. Liao, Y. Chi, Z.-T. Sie, C.-H. Ku, C.-H. Chang, M. A. Fox, P. J. Low, M.-R. Tseng and G.-H. Lee, *Inorg. Chem.,* 2015, **54**, 10811-10821.
11. V. Adamovich, S. Bajo, P.-L. T. Boudreault, M. A. Esteruelas, A. M. Lopez, J. Martín, M. Olivan, E. Oñate, A. U. Palacios, A. S. Torcuato, J.-Y. Tsai and C. Xia, *Inorg. Chem.,* 2018, **57**, 10744-10760.
12. W. T. Li, T. Z. Miao, B. W. Wang, J. X. Liu, X. Q. Lü, G. R. Fu, W. X. Feng and W.-Y. Wang, *J. Mater. Chem. C*, 2021, **9**, 8337-8344.
13. C. Shi, H. Huang, Q. X. Li, J. W. Yao, C. C. Wu, Y. B. Cao, F. X. Sun, D. G. Ma, H. Yan, C. L. Yang and A. H. Yuan, *Adv. Opt. Mater.*, 2021, **9**, 2002060.
14. M. Ibrahim-Ouali and F. Dumur, *Molecules*, 2019, **24**, 1412.
15. J. V. Caspar and T. J. Meyer, *J. Phys. Chem.*, 1983, **87**, 952-957.
16. E. Orselli, R. Q. Albuquerque, P. M. Fransen, R. Fröhlich, H. M. Janssen, L. De Cola, *J. Mater. Chem.*, 2008, **18**, 4579-4590.
17. (a) Y. H. Zhou, Q. L. Xu, H. B. Han, Y. Zhao, Y. X. Zheng, L. Zhou, J. L. Zuo, H. J. Zhang, *Adv. Opt. Mater.*, 2016, **4**, 1726-1731; (b) Z. P. Yan, K. Liao, H. B. Han, J. Su, Y. X. Zheng and J. L. Zuo, *Chem. Commun.*, 2019, **55**, 8215-8218.
18. T. Y. Li, Y. M. Jing, X. Liu, Y. Zhao, L. Shi, Z. Y. Tang, X. Y. Zheng and J. L. Zuo, *Sci. Rep.*, 2015, **5**, 14912.
19. A. B. Tamayo, B. D. Alleyne, P. I. Djurovich, S. Lamansky, I. Tsyba, N. N. Ho, R. Bau and M. E. Thompson, *J. Am. Chem. Soc.*, 2003, **125**, 7377-7387.
20. J. C. Deaton, R. H. Young, J. R. Lenhard, M. Rajeswaran and S. Huo, *Inorg. Chem.*, 2010, **49**, 9151-9161.
21. A. Heil, K. Gollnisch, M. Kleinschmidt and C. M. Marian, *Mol. Phys.*, 2016, **114**, 407-422.
22. S. Arroliga-Rocha and D. Escudero, *Inorg. Chem.*, 2018, **57**, 12106-12112.
23. E. Baranoff, S. Suárez, P. Bugnon, C. Barolo, R. Buscaino, R. Scopelliti, L. Zuppiroli, M. Graetzel and M. K. Nazeeruddin, *Inorg. Chem.*, 2008, **47**, 6575-6577.
24. W. Wei, S. A. M. Lima, P. I. Djurovich, A. Bossi, M. T. Whited and M. E. Thompson, *Polyhedron*, 2018, **140**, 138-145.
25. K.-H. Kim and J.-J. Kim, *Adv. Mater.*, 2018, **30**, 1705600.
26. M. J. Jurow, C. Mayr, T. D. Schmidt, T. Lampe, P. I. Djurovich, W. Brutting and M. E. Thompson, *Nat. Mater.*, 2016, **15**, 85-91.
27. C.-K. Moon, K.-H. Kim and J.-J. Kim, *Nat. Commun.*, 2017, **8**, 1-10.
28. I. Shigeru, Y. Shigeyuki, M. Takeshi, N. Hiroyuki, F. Hideki, K. Shiro and S. Yoshiaki, *Inorg. Chem. Commun.*, 2013, **38**, 14-19.
29. (a) Z. Chen, H. Y. Zhang, D. W. Wen, W. H. Wu, Q. G. Zeng, S. M. Chen and W.-Y. Wong, *Chem. Sci.*, 2020, **11**, 2342-2349; (b) C. F. You, D. H. Liu, J. T. Yu, H. Tian, M. B. Zhu, B. Zhang, Y. Liu, Y. F. Wang and W. G. Zhu, *Adv. Opt. Mater.*, 2020, **8**, 2000154; (c) H. U.Kim, S. Sohn, W. Choi, M. Kim, S. U. Ryu, T. Park, S. Jung and K. S. Bejoymohandas, *J. Mater. Chem. C.,* 2018, **6**, 10640-10658; (d) G. R. Fu, H. Zheng, Y. N. He, W. T. Li, X. Q. Lü and H. S. He, *J. Mater. Chem. C*, 2018, **6**, 10589-10596; (e) S. Kesarkar, W. Mróz, M. Penconi, M. Pasini, S. Destri, M. Cazzaniga, D. Ceresoli, P. R. Mussini, C. Baldoli, U. Giovanella and A. Bossi, *Angew. Chem. Int. Ed.*, 2016, **55**, 2714-2718.
30. Y. Cudré, E. F. de Carvalho, G. R. Burgess, L. Male, S. J. A. Pope, I. Tavernelli and E. Baranoff, *Inorg. Chem.*, 2017, **56**, 11565-11576.
31. D. Wasserberg, S. C. J. Meskers and R. A, J. Janssen, *J. Phys. Chem. A*, 2007, **111**, 1381-1388.
32. H. Yersin and W. J. Finkenzeller, *Highly Efficient OLEDs with Phosphorescent Materials*, Wiley-VCH: Weineim, Germany, 2008; pp 1-97.
33. D. R. Martir and E. Zysman-Colman, *Coord. Chem. Rev.*, 2018, **364**, 86-117.